Polyhedron 155 (2018) 485–492

Contents lists available at ScienceDirect

Polyhedron

journal homepage: www.elsevier.com/locate/poly

Enhancing CO_2/CH_4 and CO_2/N_2 separation performances of ZIF-8 by post-synthesis modification with [BMIM][SCN]

Muhammad Zeeshan [a,b], Seda Keskin [a,b,*], Alper Uzun [a,b,c,*]

[a] Department of Chemical and Biological Engineering, Koç University, Rumelifeneri Yolu, 34450 Sariyer, Istanbul, Turkey
[b] Koç University TÜPRAŞ Energy Center (KUTEM), Koç University, Rumelifeneri Yolu, 34450 Sariyer, Istanbul, Turkey
[c] Koç University Surface Science and Technology Center (KUYTAM), Koç University, Rumelifeneri Yolu, Sariyer, 34450 Istanbul, Turkey

ARTICLE INFO

Article history:
Received 25 May 2018
Accepted 29 August 2018
Available online 6 September 2018

Keywords:
Metal organic framework (MOF)
Ionic liquid (IL)
Incorporation
CO_2 separation
Hybrid materials

ABSTRACT

Ionic liquid (IL)-incorporated metal organic frameworks (MOFs) are promising materials for gas adsorption and separation processes. In this work, 1-*n*-butyl-3-methylimidazolium thiocyanate ([BMIM][SCN]) was incorporated in a zeolitic imidazolate framework (ZIF-8) to examine the adsorption and separation of different gases. X-ray diffraction (XRD) and scanning electron microscopy (SEM) results confirmed that ZIF-8 retains its structural integrity in the IL-incorporated sample. The Brunauer–Emmett–Teller (BET) surface area and pore volume of the IL-incorporated sample decreased significantly indicating the IL confinement into the MOF. Results of thermogravimetric analysis (TGA) demonstrate changes in the decomposition temperatures of both bulk IL and pristine ZIF-8 when the IL was incorporated into the MOF pores. Fourier transform infrared (FTIR) spectroscopy was performed to confirm the presence of interactions and successful incorporation of IL into MOF. Gas adsorption isotherms of CO_2, CH_4, and N_2 were measured for pristine ZIF-8 and IL-incorporated ZIF-8. The uptake amounts for each gas decreased as compared to their values on pristine ZIF-8, however, the decrease in the CO_2 uptake was less compared to CH_4 and N_2. The IL-incorporated sample exhibited approximately 2.6-times higher ideal selectivity for CO_2/CH_4 and four-times higher ideal selectivity for CO_2/N_2 at 1 mbar than their corresponding values for pristine ZIF-8. These results indicate that IL-MOF combinations offer a huge potential for gas separations.
© 2019 The Authors. Published by Elsevier Ltd. This is an open access article under the CC BY-NC-ND license (http://creativecommons.org/licenses/by-nc-nd/4.0/).

1. Introduction

Separation and purification of gases by nanoporous materials are broadly used in the adsorption-based processes as these processes are cost-effective, energy efficient, and environmentally friendly [1]. The widely studied nanoporous adsorbents for separation of CO_2 from CH_4 and N_2 consist of zeolites, silica gels, and carbon nanotubes. It is desired to identify a new class of nanoporous materials with enhanced separation performance for CO_2 that will lead to high CO_2/CH_4 and CO_2/N_2 selectivities. Such performance in natural gas purification and flue gas separation processes are important because they play significant roles in mitigation of CO_2 emissions. Metal organic frameworks (MOFs), crystalline structures composed of metal complexes linked by organic linkers, have been considered as promising alternatives to traditional nanoporous materials because of their large surface areas, high porosities, low densities, tunable pore sizes, and good thermal stabilities [2–4]. A large number of different kinds of MOFs has been synthesized to date and these novel materials offer a variety of structures that can be utilized in the adsorption-based separation of different gases [5–7]. Several recent reviews address the opportunities of using MOFs and MOF-based nanomaterials for CO_2 separations [8–11]. One recent approach is to modify MOF structures by some post-synthesis techniques to further improve their gas storage and separation performances. In this respect, modifying the structures with ionic liquids (ILs) offers a great degree of flexibility due to the availability of theoretically unlimited number of possible MOF and IL combinations.

ILs are salts composed of organic cations and organic or inorganic anions, which have high thermal stability and low vapor pressure. They are commonly liquid at room temperature [12,13]. Thanks to their tunable structures, they offer an almost infinite number of possible anion/cation combinations that can be utilized in different applications, such as solid phase extraction [14], catalysis [15], liquid–liquid extraction [14], and gas separation [16]. Among these applications, incorporation of ILs into MOFs holds a tremendous potential in the way of improving the performance of the bare, non-incorporated MOFs. The benefits of this approach

* Corresponding authors at: Department of Chemical and Biological Engineering, Koç University, Rumelifeneri Yolu, 34450 Sariyer, Istanbul, Turkey.
E-mail addresses: skeskin@ku.edu.tr (S. Keskin), auzun@ku.edu.tr (A. Uzun).

https://doi.org/10.1016/j.poly.2018.08.073
0277-5387/© 2019 The Authors. Published by Elsevier Ltd.
This is an open access article under the CC BY-NC-ND license (http://creativecommons.org/licenses/by-nc-nd/4.0/).

extend to various applications, such as ionic conductivity, catalysis, gas storage, and gas separation [7].

Previous studies on IL incorporated-MOF composites suggest that ILs have a positive effect especially on the gas separation performances (i.e. selectivities) of materials. For instance, our group incorporated 1-*n*-butyl-3-methylimidazolium hexafluorophosphate [BMIM][PF_6] into a zeolite imidazolate framework, ZIF-8, and CO_2/N_2 selectivity of the IL-incorporated ZIF-8 was reported to be almost three-times of the pure ZIF-8 at low pressure [17]. Similarly, when 1-*n*-butyl-3-methylimidazolium tetrafluoroborate [BMIM][BF_4] was incorporated into ZIF-8, CO_2/CH_4 and CO_2/N_2 selectivities increased from 2.2 to 4 and 6.5 to 13.4, respectively [18]. Incorporation of [BMIM][BF_4] into a different MOF, HKUST-1 ($Cu_3(BTC)_2$; BTC = benzene-1,3,5-tricarboxylate), illustrated that CH_4 selectivities over CO_2, N_2, and H_2 were improved compared to the parent MOF [19]. Mohamedali et al. incorporated two different ILs having acetate anions, [BMIM][Ac] and [EMIM][Ac], in ZIF-8. They reported an increase in the CO_2 capacity by seven-times at 30 °C, 0.1 bar, whereas the CO_2/N_2 selectivity was improved by 18-times at 50 °C and 0.1 bar compared to the corresponding values of ZIF-8 [20]. Xue et al. computationally investigated the diffusion of 1-*n*-butyl-3-methyl-imidazolium thiocyanate, [BMIM][SCN] in different MOFs, and concluded that higher gas separation performance can be achieved with better dispersion, where the dispersion was computationally characterized using the coordination numbers of the ILs in MOFs [21]. In their computational study, they reported an increase in separation of CO_2 from CH_4 and N_2 in the composite sample compared to pristine ZIF-8. This enhancement in gas adsorption and separation performance upon IL incorporation indicates the presence of direct interactions between the IL molecules and MOF. Moreover, the IL-incorporated MOF-based mixed matrix membranes (MMMs) have been recently reported, where MOFs are used as fillers while the ILs act as cavity occupants in the polymer matrices to improve the gas selectivity [22–24]. For instance, Yujie et al. synthesized a [BMIM][Tf_2N]/ZIF-8 composite and used it as a filler particle in polysulfone (PSF). Their results demonstrated that the ideal CO_2/CH_4 and CO_2/N_2 selectivities were increased by two- and four-times, respectively, in [BMIM][Tf_2N]/ZIF-8/PSF membrane compared to the bare PSF membrane [22].

Even though these early studies present a huge potential for improved performance, the field is still too new. Thus, the examples should be extended to different IL-MOF combinations to generate a firm base for the rational design of new IL/MOF composites to unlock their full potential. In this study, we incorporated 1-*n*-butyl-3-methylimidazolium thiocyanate [BMIM][SCN] into ZIF-8 (Basolite Z1200, 2-methylimidazole zinc salt). ZIF-8 was chosen as it is a robust and commercially available MOF with appropriate pore sizes for CO_2/CH_4 and CO_2/N_2 separations. We have chosen [BMIM][SCN] because previously we reported the incorporation of different ILs ([BMIM][PF_6], [BMIM][BF_4], and [HEMIM][DCA]) in ZIF-8. To be able get a better understanding on the structural factors controlling the performance of IL/MOF composites, we aimed to extend our approach to a different IL with the same cation, as used in these previous studies, having a different anion. In this way, it will be possible to compare the effect of anion type on the performance of IL/ZIF-8 composites. The IL/MOF composite was then characterized in detail using various experimental techniques. For this purpose, Fourier transform infrared (FTIR) spectroscopy, X-ray diffraction (XRD), scanning electron microscopy (SEM), Brunauer–Emmett–Teller surface area (BET), and thermogravimetric analysis (TGA) were used to check if the individual structures of the IL and the MOF remain intact and to identify any kind of interactions between them. Adsorption performances of ZIF-8 and [BMIM][SCN]/ZIF-8 composite were also measured for CO_2, CH_4, and N_2 using the volumetric gas adsorption method. The selectivities of pristine ZIF-8 and [BMIM][SCN]/ZIF-8 composite were calculated for CO_2/CH_4 and CO_2/N_2 separations and compared with each other to identify the possible reasons for the performance enhancement. Results presented here provide a deeper level understanding for the selection of proper components for these IL/MOF composites, a fairly new family of materials, of which very little is currently known for rational design.

2. Experimental section

2.1. Materials and sample preparation

ZIF-8 (Basolite Z1200, 2-methylimidazole zinc salt), [BMIM][SCN], and acetone were purchased from Sigma-Aldrich at the highest available purity level and stored in an Ar-filled glovebox (Labconco). N_2 (99.998 vol%), CH_4 (99.95 vol%), and CO_2 (99.9 vol %) used for gas adsorption measurements were acquired from Linde gas company. The IL-incorporated sample was prepared by wet impregnation, as reported previously [17,19,25]. To remove the moisture content and other volatile impurities from ZIF-8, it was first dehydrated at 105 °C overnight in a vacuum oven. To prepare a 30 wt% IL-incorporated composite, first 300 mg of [BMIM][SCN] was dissolved in approximately 20 mL of acetone and continuously stirred for 1 h at room temperature. To avoid the acetone evaporation, the sample container was covered with paraffin while stirring. Then, 700 mg of activated ZIF-8 was added to the solution followed by continuous stirring for 6 h at 30 °C in open atmosphere to slowly evaporate the acetone. Once the acetone was completely evaporated, the sample was put in an oven for overnight at 105 °C to completely dry the sample. The resultant sample was stored in a desiccator before use.

2.2. Characterization and performance measurement

2.2.1. Scanning electron microscopy (SEM)

The surface features and morphologies of the pristine ZIF-8 and [BMIM][SCN]/ZIF-8 were investigated by a Zeiss Ultra Plus Field emission scanning electron microscope. For scanning the samples, a voltage of 3 kV was applied under ultra-high vacuum at the corresponding working distances of 4.8 and 4.3 mm for ZIF-8 and [BMIM][SCN]/ZIF-8, respectively. Images were obtained at two different magnifications (100 k× and 10 k×).

2.2.2. X-ray diffraction (XRD)

The XRD pattern for ZIF-8 and [BMIM][SCN]/ZIF-8 were obtained by a Bruker D8 advance X-ray diffraction system with a Cu Kα1 radiation source using a wavelength of 1.54 Å. The power rating of X-ray generator was set to 30 kV of voltage and 10 mA of current, and Lynxeye detector with a slit size of 1 mm was used. The diffraction patterns were collected in a range of 2θ values of 5–45°, with a step size of 0.0204°.

2.2.3. Brunauer–Emmet–Teller (BET) analysis

A Micromeritics ASAP 2020 physisorption analyzer was used to perform the BET analyses of ZIF-8 and the composite sample. For each analysis, approximately 150 mg of sample was used. Prior to each measurement, the samples were degassed and activated at 125 °C under vacuum for overnight. Following the activation, free space measurement of samples was performed using helium gas at liquid nitrogen temperature of 77 K. N_2 gas adsorption isotherm was obtained between 10^{-6} and 1 bar, and the pressure steps between 0.05 and 0.3 bar were used in BET equation to estimate the surface areas of samples.

2.2.4. Thermogravimetric analysis (TGA)

Thermogravimetric analyses were carried out to determine the thermal stability of pristine ZIF-8, bulk [BMIM][SCN], and [BMIM][SCN]/ZIF-8 composite on a TA Instruments Q500 model thermogravimetric analyzer using a platinum pan. After tarring, approximately 15 mg of each sample was placed in the pan. At first, for each sample, a constant heating rate of 5 °C/min was employed up to 120 °C followed by an isothermal treatment for 8 h at the same temperature. Under a continuous N_2 flow of 40 mL/min and 60 mL/min for balance and purge gases, respectively, the sample temperature was then raised to 700 °C at a ramp rate of 2 °C/min. For comparing the thermal decomposition temperatures, onset (T_{onset}) and derivative onset (T'_{onset}) temperatures were determined from thermogravimetry (TG) and derivative gravimetric (DTG) curves. In this study, we used T'_{onset} thermal decomposition temperature, as T_{onset} values mostly overestimates the decomposition temperature [15,26].

2.2.5. Fourier transform infrared (FTIR) spectroscopy

The FTIR spectra of the bulk IL, pristine ZIF-8, and the composite sample were obtained by using a Thermo Scientific Nicolet iS50 model FTIR spectrometer with an attenuated total reflection cell. The IR spectra was obtained in transmission mode between the range of 3400 and 400 cm^{-1} with 64 and 512 scans of background and sample scan, respectively, while the resolution was set to 2 cm^{-1} for each sample. Deconvolution of the IR bands was performed using the Fityk software by employing the Voigt function [27].

2.2.6. X-ray fluorescence (XRF) spectroscopy

A Bruker S8 Tiger XRF spectrometer was used to perform elemental analysis for ZIF-8 and [BMIM][SCN]/ZIF-8 sample. Under helium atmosphere, a 4 kW Rh anode X-ray tube was used to generate X-rays. For each sample, the XRF sample container (Chemplex Industries Inc.) was filled with approximately 150 mg powder sample, and a 4 μm Prolene film support (Chemplex Industries Inc.) was placed on top of the container. The film was then immobilized with a ring. The common ppm level impurities for almost all samples were found to be Ca, P, Fe, Zn, Cu, Zr, Ti, and Al. Data interpretation of samples was performed by using the SpectraPlus Eval2 V2.2.454 software.

2.2.7. High-Pressure volumetric adsorption (HPVA) analysis

A Micromeritics (Particulate Systems) High-Pressure Volumetric Analyzer HPVA II-200 was used to perform gas adsorption measurement of samples [28]. Adsorption isotherms of CO_2, CH_4, and N_2 were measured for pristine ZIF-8 and [BMIM][SCN]/ZIF-8 sample. Approximately 400 mg of sample was weighed and loaded into a sample holder. Each sample was first activated in a degas port prior to the measurements. For this purpose, the samples were degassed overnight at 125 °C under vacuum until the pressure reached to 10^{-6} bar. After activation, the sealed sample holder was connected to the analysis port. Before starting the analysis, unwanted residuals from the previous experiment were cleaned by purging all lines of the system three times with helium gas. Adsorption isotherms of CO_2, CH_4, and N_2 gases were acquired up to 1000 mbar at a temperature of 25 °C. The obtained gas adsorption isotherm of CO_2, and CH_4 were fitted to the dual-site Langmuir model and N_2 gas adsorption isotherm was fitted to dual-site Langmuir-Freundlich model. Fitted parameters of these models are given in Table S1, experimental and fitted gas adsorption isotherms are demonstrated in Fig. S1. Ideal CO_2/CH_4 and CO_2/N_2 selectivities of the samples were calculated by dividing the uptake values of gases at the same pressures.

3. Results and discussion

The [BMIM][SCN]-incorporated ZIF-8 sample was prepared at an IL loading of approximately 30 wt%, as reported previously (trials at an IL loading higher than 30 wt% exceeded the wetness point and led to mud formation) [19]. In one of our previous works [18], different IL loadings were tried and changes in gas uptakes with respect to IL loadings were reported. As the IL loading increased, a higher degree of decrease in gas uptakes is expected because of a decrease in the available pore space of MOF. The maximum difference in gas uptakes was found at 30 wt% IL loading leading to the highest selectivity improvement. Therefore, the maximum achievable IL loading was used in this work to obtain the highest selectivity improvement. Once the composite sample was prepared, detailed characterization was performed to confirm (i) successful incorporation of IL into the ZIF-8 pores, (ii) the structural integrity of ZIF-8, and (iii) the presence of any interactions between IL and ZIF-8.

To confirm the IL loading in the composite sample, XRF measurements were performed. Based on the data given in Table 1, the calculated IL amount was found to be approximately 25 wt%. The difference in stoichiometric IL loading versus calculated amount can be attributed to the amount of IL lost on the walls of the sample container during the sample preparation. Moreover, the BET measurements presented in Fig. S2 support these observations and indicate that the surface area and pore volume of the pristine ZIF-8 reduced from 1208 m^2/g and 0.63 cm^3/g to 60.56 m^2/g and 0.027 cm^3/g in composite sample, respectively. The difference between the pore volumes of the pristine MOF and IL/MOF composite indicates that IL loading is approximately 26 wt% (assuming that the density of the IL is the same when confined in the MOF), almost consistent with the XRF results. Considering the XRF results provide a more direct evidence on the amount of IL, and the density of IL might be slightly different when confined in the nano-sized pores [29], we conclude that the IL loading was approximately 25 wt%.

Fig. 1 illustrates the surface morphology of ZIF-8 and IL-incorporated ZIF-8 sample. These SEM images of the composite clearly indicate that the rhombic dodecahedron ZIF-8 structure was intact after the IL incorporation [30]. These results are consistent with the XRD results presented in Fig. 2. IL/ZIF-8 composite demonstrates changes only on the intensity of some of the features as compared to the pristine ZIF-8. Other than these intensity changes, positions of the XRD features of the ZIF-8 remain unchanged upon IL incorporation. Changes in the intensities can be attributed to the possible changes in the electronic environment of the composite because of the presence of IL in the ZIF-8 cages [20,22].

Results of the TGA measurements on the pristine ZIF-8, bulk IL, and the composite sample are presented in Fig. 3. The values for T'_{onset} of the pristine ZIF-8 and bulk IL were found to be 375 and 221 °C, respectively, in good agreement with the literature [31]. However, results demonstrate that after the incorporation of [BMIM][SCN] into ZIF-8, thermal stability of the composite decreased to 200 °C as illustrated in Table 2. Similar kind of decrease was also reported previously on [BMIM][BF_4] and [BMIM][PF_6]-incorporated ZIF-8 and on imidazolium-type ILs

Table 1
Zn and S amount in the IL/ZIF-8 sample determined by XRF measurement.

Formula	Concentration (wt %)
CHN	80.9
Zn	15.9
S	3.0
impurities	0.02

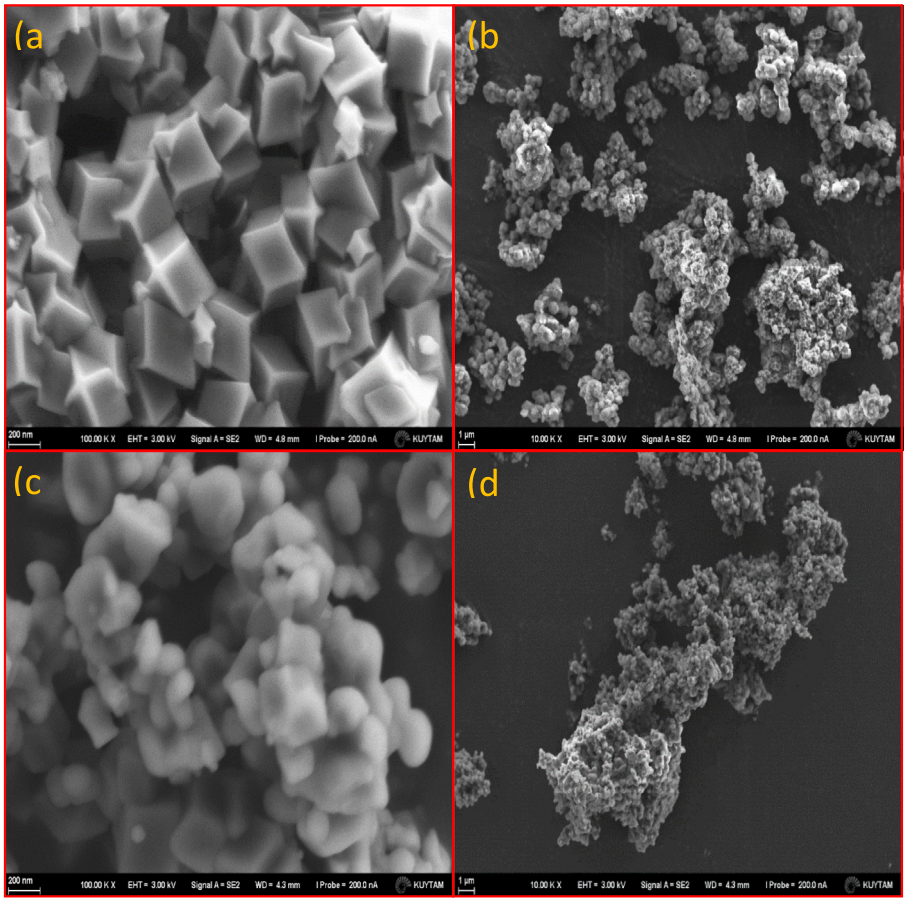


Fig. 1. Morphology of (a, b) ZIF-8 and (c, d) [BMIM][SCN]/ZIF-8 at 100 k× and 10 k×.

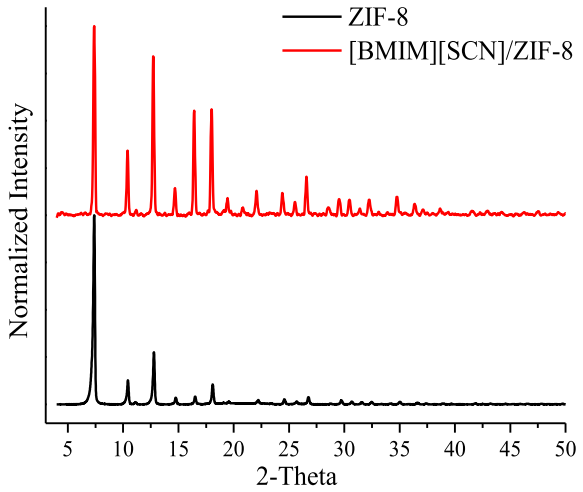


Fig. 2. XRD patterns of ZIF-8 with those of [BMIM][SCN]/ZIF-8 composite.

supported on various metal oxides [15,17,18,20,32]. Data in Fig. 3 also indicate that thermal decomposition does not occur in a single step as in the case of pristine ZIF-8 and bulk IL. The first peak occurring at 100 °C in bulk IL and composite sample can be attributed to the loss of moisture content.

A major decomposition peak was observed in the composite at 200 °C, which is approximately 20 °C lower than that of the bulk IL. This decrease in the decomposition temperature indicates the presence of interactions between the IL and MOF, playing a role in the decomposition mechanism. Because of the presence of these interactions, it is followed by a second decomposition step at a relatively higher temperature. Such kind of interactions were also evidenced by the amount of sample remained after the TGA measurement was completed. The results illustrate that bulk IL disappears entirely before the temperature reaches to 330 °C, while ZIF-8 losses approximately 40 wt% of its initial mass, when the temperature reaches to 700 °C. The IL loading calculated from XRF and BET measurements was approximately 25 wt% and based on this value one can expect to see that the composite shows a loss of approximately 55 wt% at 700 °C [20]. However, at 700 °C in the IL-incorporated composite, this amount increased to approximately 60 wt%, which is more than the expected value. From this observation, it can be inferred that while IL was decomposing and leaving the MOF, it also causes decomposition of the framework confirming the presence of interactions between the IL and MOF [33].

To further identify these interactions, FTIR spectra of pristine ZIF-8, bulk [BMIM][SCN], and [BMIM][SCN]/ZIF-8 were measured and shown in Fig. 4. The presence of the IR bands associated with the bulk [BMIM][SCN] in the composite sample indicates successful incorporation of IL into the MOF. To understand the interactions, the IR bands were analyzed in detail and changes in the positions of bands were examined. To highlight these peaks, the IR data were divided into two different frequency regions of 400–2150 cm^{-1} and 2800–3200 cm^{-1}. First, the peaks were deconvoluted and then the shifts in peaks position were analyzed by considering the corresponding peak positions in bulk IL.

Table 3 and Fig. 4 illustrate that the IR spectra of the composite showing changes in peak positions and intensities of the IR

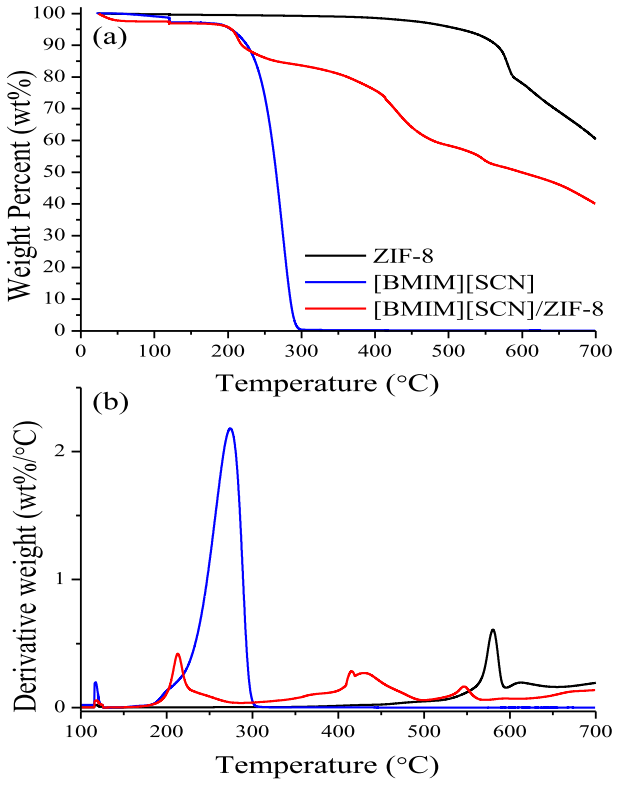


Fig. 3. TGA plots of pristine ZIF-8, [BMIM][SCN], and [BMIM][SCN]/ZIF-8 composite. (a) Change of weight percent with temperature and (b) change of derivative weight percent with temperature.

Table 2
T_{onset} derivative decomposition temperature of pristine ZIF-8, [BMIM][SCN], and [BMIM][SCN]/ZIF-8.

Sample	T_{onset} (°C)
ZIF-8	375
[BMIM][SCN]	221
[BMIM][SCN]/ZIF-8	200

features belonging mostly to the IL. The bands at 3144, 3092, 3107, and 2959 cm^{-1} exhibited a blue shift of 4, 3, 7, and 3 cm^{-1}, respectively, (slightly higher than our spectral resolution) in the composite sample indicating an increase in the C–H stretching or bending vibrations in butyl groups and the imidazolium ring itself. The strong band assigned to C–N stretching mode in bulk IL at 2047 cm^{-1} had a major blue shift to 2054 cm^{-1} in the composite. This band corresponds to C≡N stretching vibration of the thiocyanate group of the IL's anion. This shift indicates a change in the electronic distribution between the anion and MOF, confirming the presence of interactions between these two components. Also, the band at 1464 cm^{-1} for C=N stretching exhibits a red shift to 1457 cm^{-1}. The band at 840 cm^{-1} corresponding to C–S stretching vibration, on the other hand, had a blue shift of 8 cm^{-1}. As the major shifts in the peak positions were observed in the bands assigned to the anion part of IL, it can be inferred that after the incorporation, $[SCN]^-$ is interacting more with the imidazolate groups of the ZIF-8 rather than its counter ion $[BMIM]^+$ as evidenced by strengthening of the corresponding bonds, indicated by blue shifts on the band positions.

As the detailed characterization confirms the presence of interactions between the IL and the MOF, one can expect that these interactions have a direct influence on the gas adsorption and separation performance of the samples. To determine the gas adsorption performance of the composite, volumetric adsorption of CO_2, CH_4, and N_2 gases were measured up to 1000 mbar at 25 °C. Results of these adsorption isotherm measurements for different gases in pristine ZIF-8 and composite sample are presented in Fig. 5.

Results presented in Fig. 5(d) illustrate a decrease in gas uptakes of composite as compared to the pristine ZIF-8 throughout the entire pressure range up to 1000 mbar. However, the amount of decrease in uptakes are different for each gas. For instance, CO_2, CH_4, and N_2 uptakes decrease to approximately 66%, 25%, and 16% of their corresponding values in pristine MOF at a low

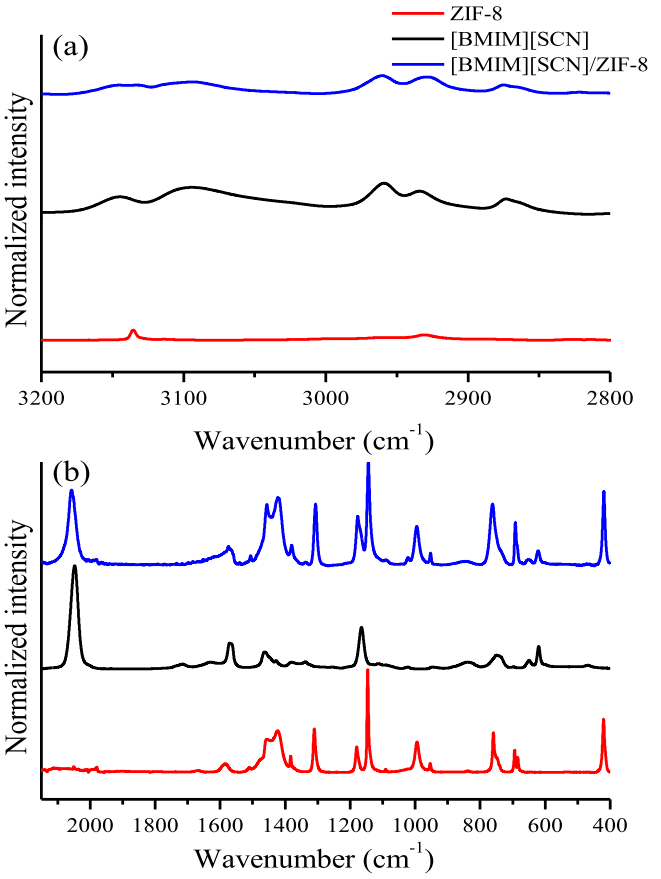


Fig. 4. FTIR spectra of pristine ZIF-8, bulk [BMIM][SCN], and [BMIM][SCN]/ZIF-8 in two different regions: (a) 2800–3200 cm^{-1} and (b) 400–2150 cm^{-1}.

Table 3
Shift in FTIR bands of bulk IL upon incorporation into ZIF-8.

Assignment*	Bulk IL (exp.)	IL-incorporated ZIF-8 (exp.)
Ring ν(C4–C5H)$_{asym}$ [33]	3146	3148
Ring ν(C2H)$_{sym}$ [33]	3092	3095
Ring ν(CH$_3$)$_{asym}$ [33]	3107	3114
Butyl ν(HC1HH)$_{sym}$, ν(HC2H)$_{asym}$ [33]	2959	2962
Butyl ν(HC1H)$_{sym}$, ν(HC2H)$_{sym}$, ν(HC3H)$_{asym}$, ν(HC4HH)$_{sym}$ [33]	2874	2876
ν(C–N) [34]	2047	2054
Ring δ(C2H), Ring CH$_3$ δ(HCH) scissoring, Ring ν(C2–N) [33]	1572	1574
ν(C=N) [34]	1464	1457
Ring in plane asym stretch, Butyl δ(HC1H) twisting [33]	1426	1421
ν(C–S) [34]	840	848

* ν: stretching, δ: bending.

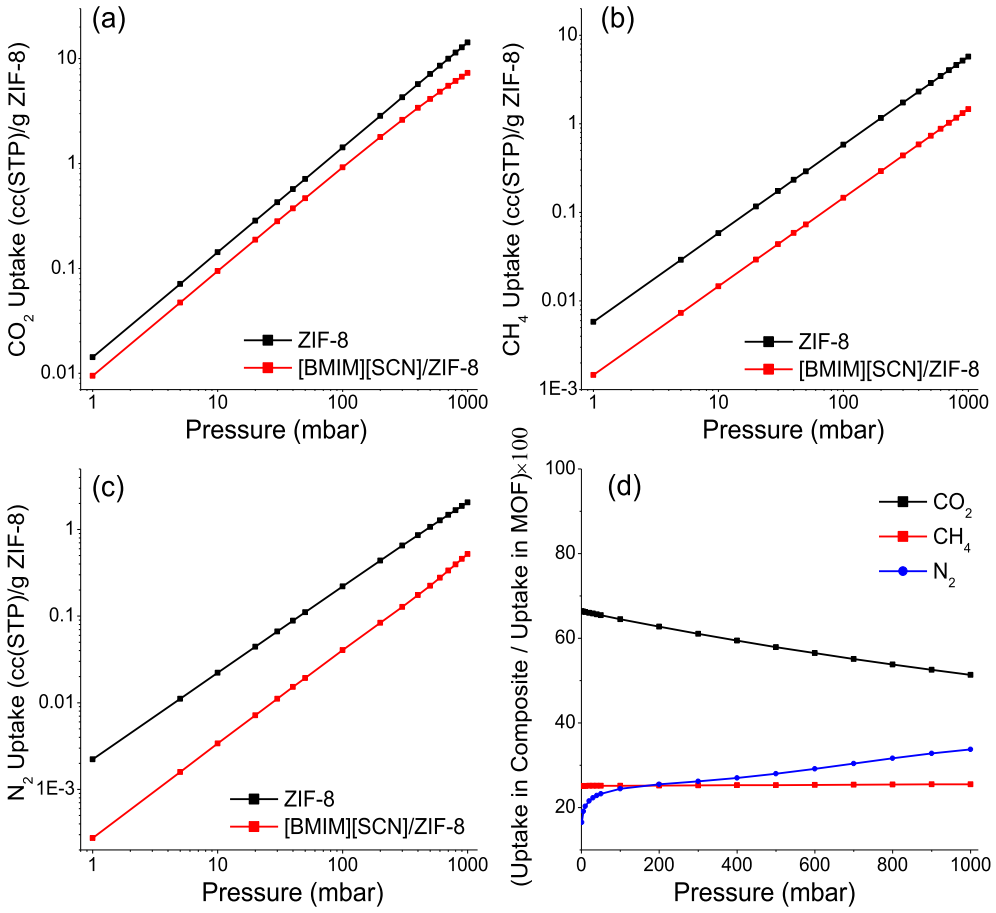


Fig. 5. (a) CO_2 (b) CH_4 (c) N_2 uptakes of pristine ZIF-8 and [BMIM][SCN]/ZIF-8 at room temperature, (d) change in the uptakes values of gases upon IL incorporation.

pressure of 1 mbar, respectively. These changes in uptakes can be associated with a decrease in the surface area and pore volume of composite compared to the parent MOF caused by the incorporation of the IL. However, the IL-MOF interactions in the composite may also a play a role in determining the variations in uptake performance. They can either modify the previously existing sites or may create new sites for gas adsorption. Because the available pore volume is mostly important at high pressures, we infer that at these low pressures the interactions between the adsorbate and composite become the dominant factor in determining the gas uptake performance. The lower decrease in CO_2 uptake compared to those in CH_4 and N_2 can be related to the differences in the interactions between CO_2 and [BMIM][SCN]/ZIF-8 composite associated with high quadrupole moment of CO_2 which facilitates efficient adsorption at low pressures [25,35,36]. The different levels of changes in gas uptake performances observed upon the incorporation of the IL suggest that the gas separation performance of the composite would also change.

Fig. 6a and b show the ideal CO_2/CH_4 and CO_2/N_2 selectivities together with those calculated by Ideal Adsorption Solution Theory

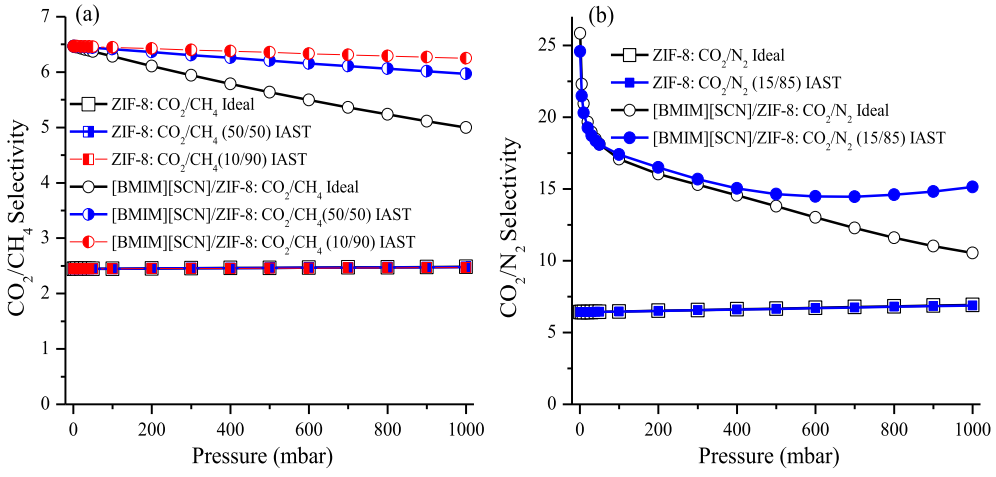


Fig. 6. Ideal selectivities and IAST-predicted mixture selectivities of pristine ZIF-8 and [BMIM][SCN]/ZIF-8 samples for (a) CO_2/CH_4 (b) CO_2/N_2 separations.

(IAST) for pristine ZIF-8 and [BMIM][SCN]/ZIF-8. Ideal selectivity generally gives an idea about the materials' separation performances, however, gases exist as a mixture in a real process. Therefore, we computed IAST selectivities [37] to make an assessment about the mixture separation performance of the composite. Previous reports discussed that IAST accurately predicts selectivities of MOFs in different gas compositions [38–41].

According to Fig. 6(a), the ideal CO_2/CH_4 selectivity at 1 mbar exhibits an increase of 2.6-times compared to pristine ZIF-8. As the pressure increases, this increase in selectivity tends to decrease however, at a pressure of 1000 mbar, increase in selectivity remains twice of the composite relative to the selectivity of pristine ZIF-8. Our findings agree with the computational work of Xue et al. who reported two-times increase in CO_2/CH_4 (10/90) selectivity [21]. Our IAST prediction for CO_2/CH_4 (10/90) selectivity is 5.96, while molecular simulations reported a selectivity of 6.25 [21]. We observed a more prominent increase for CO_2/N_2 selectivity of the IL-impregnated sample as shown in Fig. 6(b). Both ideal and mixture selectivities were found to be approximately four-times higher than their counterparts in pristine ZIF-8 at low pressures. These improvements in CO_2/CH_4 and CO_2/N_2 separation performance illustrate that [BMIM][SCN]-incorporated ZIF-8 can be a promising alternative for CO_2 separation process.

4. Conclusion

In this study, we successfully incorporated [BMIM][SCN] in one of the robust and most studied MOFs, ZIF-8, to investigate the consequences of IL incorporation on the gas uptakes and selectivities of ZIF-8. Several characterization techniques, such as XRD, XRF, SEM, BET, FTIR spectroscopy, and TGA were used to analyze the IL-MOF composite. XRD and SEM results confirmed that ZIF-8 keeps its integrity after the IL incorporation. Furthermore, BET results show a decrease in the surface area and pore volume of composite sample compared to the pristine ZIF-8, which further confirmed that IL was successfully incorporated into ZIF-8. TGA results indicate that the decomposition mechanism changes for the composite sample because of the interactions as compared to bulk IL and pristine ZIF-8. Such interactions were further confirmed by the IR results, which show the shifts in peak positions of IR features of the IL's anion in the composite sample. To investigate the effects of these interactions on the gas uptakes and selectivities, volumetric adsorption of CO_2, CH_4, and N_2 were measured for the pristine ZIF-8 and the composite. Data illustrated that the gas uptakes decreased in the composite sample compared to the corresponding values in pristine ZIF-8, however, the decrease in uptakes is different for each gas. Because of this difference, the separation performance was significantly improved in IL-incorporated ZIF-8 sample. At relatively low pressures, the ideal selectivities of CO_2/CH_4 and CO_2/N_2 were improved 2.6 and four-times as compared to its values in pristine ZIF-8. The results presented in this study indicate that the IL-MOF combinations offer a huge potential to design hybrid materials that can a play a vital role in gas adsorption and separation applications.

Acknowledgements

This work is supported by the Scientific and Technological Research Council of Turkey (TUBITAK) under 1001-Scientific and Technological Research Projects Funding Program (project number: 114R093) and by Koç University Seed Fund Program. Support provided by the KUTEM (Koç University TÜPRAŞ Energy Center) is gratefully acknowledged. A.U. acknowledges the TUBA-GEBIP Award. S.K. acknowledges ERC-2017-Starting Grant, grant agreement No 756489-COSMOS. Support of Vahid Nozari and Çiğdem Altıntaş are gratefully acknowledged. Authors thank Koç University Surface Science and Technology Center (KUYTAM) for providing help with the sample characterization. Authors would like to thank TARLA for the collaborative research support.

Appendix A. Supplementary data

Supplementary data associated with this article can be found, in the online version, at https://doi.org/10.1016/j.poly.2018.08.073.

References

[1] R.T. Yang, Gas Separation by Adsorption Processes, Butterworths, 1987.
[2] H.C. Zhou, J.R. Long, O.M. Yaghi, Introduction to metal-organic frameworks, Chem. Rev. 112 (2012) 673, https://doi.org/10.1021/cr300014x.
[3] H. Furukawa, K.E. Cordova, M. O'Keeffe, O.M. Yaghi, The chemistry and applications of metal-organic frameworks, Science (80-) 341 (2013), https://doi.org/10.1126/science.1230444.
[4] S. Qiu, M. Xue, G. Zhu, Metal–organic framework membranes: from synthesis to separation application, Chem. Soc. Rev. 43 (2014) 6116, https://doi.org/10.1039/C4CS00159A.
[5] S.T. Meek, J.A. Greathouse, M.D. Allendorf, Metal-organic frameworks: a rapidly growing class of versatile nanoporous materials, Adv. Mater. 23 (2011) 249, https://doi.org/10.1002/adma.201002854.
[6] A. Uzun, S. Keskin, Site characteristics in metal organic frameworks for gas adsorption, Prog. Surf. Sci. 89 (2014) 56, https://doi.org/10.1016/j.progsurf.2013.11.001.
[7] F.P. Kinik, A. Uzun, S. Keskin, Ionic liquid/metal–organic framework composites: from synthesis to applications, ChemSusChem 10 (2017) 2842, https://doi.org/10.1002/cssc.201700716.
[8] H. Li, K. Wang, Y. Sun, C.T. Lollar, J. Li, H.C. Zhou, Recent advances in gas storage and separation using metal–organic frameworks, Mater. Today 21 (2018) 108, https://doi.org/10.1016/j.mattod.2017.07.006.
[9] K. Sumida, D.L. Rogow, J.A. Mason, T.M. McDonald, E.D. Bloch, Z.R. Herm, T.H. Bae, J.R. Long, Carbon dioxide capture in metal-organic frameworks, Chem. Rev. 112 (2012) 724, https://doi.org/10.1021/cr2003272.
[10] J. Yu, L.-H. Xie, J.-R. Li, Y. Ma, J.M. Seminario, P.B. Balbuena, CO_2 capture and separations using MOFs: computational and experimental studies, Chem. Rev. 117 (2017) 9674, https://doi.org/10.1021/acs.chemrev.6b00626.
[11] S.D. Kenarsari, D. Yang, G. Jiang, S. Zhang, J. Wang, A.G. Russell, Q. Wei, M. Fan, Review of recent advances in carbon dioxide separation and capture, RSC Adv. 3 (2013) 22739, https://doi.org/10.1039/c3ra43965h.
[12] K.N. Marsh, J.A. Boxall, R. Lichtenthaler, Room temperature ionic liquids and their mixtures – a review, Fluid Phase Equilib. 219 (2004) 93, https://doi.org/10.1016/j.fluid.2004.02.003.
[13] R.D. Rogers, K.R. Seddon, Ionic liquids solvents of the future, Science (80-) 302 (2003) 792, https://doi.org/10.1126/science.1090313.
[14] L. Vidal, M.L. Riekkola, A. Canals, Ionic liquid-modified materials for solid-phase extraction and separation: a review, Anal. Chim. Acta 715 (2012) 19, https://doi.org/10.1016/j.aca.2011.11.050.
[15] A. Akçay, M. Babucci, V. Balci, A. Uzun, A model to predict maximum tolerable temperatures of metal-oxide-supported 1-n-butyl-3-methylimidazolium based ionic liquids, Chem. Eng. Sci. 123 (2015) 588, https://doi.org/10.1016/j.ces.2014.11.038.
[16] E.D. Bates, R.D. Mayton, I. Ntai, J.H. Davis, CO_2 capture by a task-specific ionic liquid, J. Am. Chem. Soc. 124 (2002) 926, https://doi.org/10.1021/ja017593d.
[17] F.P. Kinik, C. Altintas, V. Balci, B. Koyuturk, A. Uzun, S. Keskin, [BMIM][PF_6] incorporation doubles CO_2 selectivity of ZIF-8: elucidation of interactions and their consequences on performance, ACS Appl. Mater. Interfaces 8 (2016) 30992, https://doi.org/10.1021/acsami.6b11087.
[18] B. Koyuturk, C. Altintas, F.P. Kinik, S. Keskin, A. Uzun, Improving gas separation performance of ZIF-8 by [BMIM][BF_4] incorporation: interactions and their consequences on performance, J. Phys. Chem. C. 121 (2017) 10370, https://doi.org/10.1021/acs.jpcc.7b00848.
[19] K.B. Sezginel, S. Keskin, A. Uzun, Tuning the gas separation performance of CuBTC by ionic liquid incorporation, Langmuir 32 (2016) 1139, https://doi.org/10.1021/acs.langmuir.5b04123.
[20] M. Mohamedali, H. Ibrahim, A. Henni, Incorporation of acetate-based ionic liquids into a zeolitic imidazolate framework (ZIF-8) as efficient sorbents for carbon dioxide capture, Chem. Eng. J. 334 (2018) 817, https://doi.org/10.1016/j.cej.2017.10.104.
[21] W. Xue, Z. Li, H. Huang, Q. Yang, D. Liu, Q. Xu, C. Zhong, Effects of ionic liquid dispersion in metal-organic frameworks and covalent organic frameworks on CO_2 capture: a computational study, Chem. Eng. Sci. 140 (2016) 1, https://doi.org/10.1016/j.ces.2015.10.003.
[22] Y. Ban, Z. Li, Y. Li, Y. Peng, H. Jin, W. Jiao, A. Guo, P. Wang, Q. Yang, C. Zhong, W. Yang, Confinement of ionic liquids in nanocages: tailoring the molecular sieving properties of ZIF-8 for membrane-based CO_2 capture, Angew. Chem., Int. Ed. 54 (2015) 15483, https://doi.org/10.1002/anie.201505508.
[23] C. Casado-Coterillo, A. Fernández-Barquín, B. Zornoza, C. Téllez, J. Coronas, Á. Irabien, Synthesis and characterisation of MOF/ionic liquid/chitosan mixed

matrix membranes for CO_2/N_2 separation, RSC Adv. 5 (2015) 102350, https://doi.org/10.1039/C5RA19331A.
[24] J. Ma, Y. Ying, X. Guo, H. Huang, D. Liu, C. Zhong, Fabrication of mixed-matrix membrane containing metal–organic framework composite with task-specific ionic liquid for efficient CO_2 separation, J. Mater. Chem. A 4 (2016) 7281, https://doi.org/10.1039/C6TA02611G.
[25] V. Nozari, S. Keskin, A. Uzun, Toward rational design of ionic liquid/metal-organic framework composites: effects of interionic interaction energy, ACS Omega 2 (2017) 6613, https://doi.org/10.1021/acsomega.7b01074.
[26] A. Akçay, V. Balci, A. Uzun, Structural factors controlling thermal stability of imidazolium ionic liquids with 1-n-butyl-3-methylimidazolium cation on γ-Al_2O_3, Thermochim. Acta 589 (2014) 131, https://doi.org/10.1016/j.tca.2014.05.018.
[27] M. Wojdyr, Fityk: a general-purpose peak fitting program, J. Appl. Crystallogr. 43 (2010) 1126, https://doi.org/10.1107/S0021889810030499.
[28] HPVA II – High Pressure Volumetric Analyzer|Particulate Systems, (n.d.). http://www.particulatesystems.com/hpva2/ (accessed 07.05.18).
[29] C. Iacob, J.R. Sangoro, W.K. Kipnusu, R. Valiullin, J. Kärger, F. Kremer, Enhanced charge transport in nano-confined ionic liquids, Soft Matter. 8 (2012) 289, https://doi.org/10.1039/C1SM06581E.
[30] M. Jian, B. Liu, R. Liu, J. Qu, H. Wang, X. Zhang, Water-based synthesis of zeolitic imidazolate framework-8 with high morphology level at room temperature, RSC Adv. 5 (2015) 48433, https://doi.org/10.1039/C5RA04033G.
[31] P. Navarro, M. Larriba, E. Rojo, J. García, F. Rodríguez, Thermal properties of cyano-based ionic liquids, J. Chem. Eng. Data 58 (2013) 2187, https://doi.org/10.1021/je400140n.
[32] M. Babucci, A. Akçay, V. Balci, A. Uzun, Thermal stability limits of imidazolium ionic liquids immobilized on metal-oxides, Langmuir 31 (2015) 9163, https://doi.org/10.1021/acs.langmuir.5b02519.
[33] M. Babucci, V. Balci, A. Akçay, A. Uzun, Interactions of [BMIM][BF_4] with metal oxides and their consequences on stability limits, J. Phys. Chem. C 120 (2016) 20089, https://doi.org/10.1021/acs.jpcc.6b03975.
[34] S.A. Dharaskar, K.L. Wasewar, M.N. Varma, D.Z. Shende, Synthesis, characterization, and application of 1-butyl-3-methylimidazolium thiocyanate for extractive desulfurization of liquid fuel, Environ. Sci. Pollut. Res. 23 (2016) 9284, https://doi.org/10.1007/s11356-015-4945-1.
[35] S. Salehi, M. Anbia, High CO_2 adsorption capacity and CO_2/CH_4 selectivity by nanocomposites of MOF-199, Energy Fuels 31 (2017) 5376, https://doi.org/10.1021/acs.energyfuels.6b03347.
[36] M. Oschatz, M. Antonietti, A search for selectivity to enable CO_2 capture with porous adsorbents, Energy Environ. Sci. 11 (2017) 57, https://doi.org/10.1039/C7EE02110K.
[37] S. Lee, J.H. Lee, J. Kim, User-friendly graphical user interface software for ideal adsorbed solution theory calculations, Korean J. Chem. Eng. 35 (2018) 214, https://doi.org/10.1007/s11814-017-0269-9.
[38] S. Keskin, Atomistic simulations for adsorption, diffusion, and separation of gas mixtures in zeolite imidazolate frameworks, J. Phys. Chem. C 115 (2011) 800, https://doi.org/10.1021/jp109743e.
[39] J. McEwen, J.D. Hayman, A. Ozgur Yazaydin, A comparative study of CO_2, CH_4 and N_2 adsorption in ZIF-8, Zeolite-13X and BPL activated carbon, Chem. Phys. 412 (2013) 72, https://doi.org/10.1016/j.chemphys.2012.12.012.
[40] Z. Zhang, S. Xian, Q. Xia, H. Wang, Z. Li, J. Li, Enhancement of CO_2 adsorption and CO_2/N_2 selectivity on ZIF-8 via postsynthetic modification, AIChE J. 59 (2013) 2195, https://doi.org/10.1002/aic.13970.
[41] M. Zeeshan, V. Nozari, M.B. Yagci, T. Isık, U. Unal, V. Ortalan, S. Keskin, A. Uzun, Core-Shell Type Ionic Liquid/Metal Organic Framework Composite: An Exceptionally High CO_2/CH_4 Selectivity, J. Am. Chem. Soc. 140 (2018) 10113, https://doi.org/10.1021/jacs.8b05802.